

Influence of phase transformations on lateral heterogeneity and dynamics in Earth's mantle

Lars Stixrude*, Carolina Lithgow-Bertelloni¹

Department of Geological Sciences, University of Michigan, Ann Arbor, MI 48109-1005, United States

Received 14 February 2007; received in revised form 14 August 2007; accepted 25 August 2007

Available online 8 September 2007

Editor: G.D. Price

Abstract

Using a self-consistent computation of phase equilibria and physical properties, we determine isobaric velocity–temperature and velocity–density scalings as a function of depth, focusing on the upper 800 km. The scalings contain an isomorphic part due to the influence of temperature on the physical properties of individual phases, and a metamorphic part due to variation of phase abundances and compositions with temperature. We show that the contribution from phase transformations is comparable in magnitude to that of temperature alone, and has important consequences for mantle structure. Both scalings are highly non-linear functions of temperature and depth even in the elastic limit due to the influence of phase transitions: near sharp phase transitions seismic velocities become much more sensitive to temperature. We expect the magnitude of lateral variations in seismic velocity to vary rapidly with depth. This result has important implications for the interpretation of smoothed tomographic models, particularly in the upper 1000 km, and possibly the bottom few hundred km, where phase transformations have a large influence on the structure. It will be important to include the metamorphic contribution of the scalings in geodynamical studies relating seismic structure to thermal structure or the gravity field. We find that the combined phase buoyancy of transitions near 520 km depth is equal in magnitude to that of the olivine to wadsleyite transition and should be included in future dynamical studies.

© 2007 Elsevier B.V. All rights reserved.

Keywords: mantle; thermodynamics; high pressure

1. Introduction

Below the lithosphere, Earth structure is approximately spherically symmetric and physical properties depend most strongly on depth. Deviations from radial structure, that is variations in physical properties with

latitude and longitude at a given depth, while small, are disproportionately important in our understanding of Earth's dynamics and evolution. For example, lateral variations in density drive mantle flow and plate motions and produce dynamic topography and the non-hydrostatic part of the geoid and gravity field. Seismic wave velocities vary laterally and the results of seismic tomography are providing us with an increasingly clear and robust view of three-dimensional mantle structure.

With advances in seismic tomography and mineral physics, particularly knowledge of the elastic properties

* Corresponding author. Now at: Department of Earth Sciences, University College London, Gower Street, London, WC1E 6BT, United Kingdom.

E-mail address: stixrude@umich.edu (L. Stixrude).

¹ Now at: Department of Earth Sciences, University College London, Gower Street, London, WC1E 6BT, United Kingdom.

of mantle phases at high pressure and temperature, has come an increasing interest in the origins of lateral heterogeneity. Much of the lateral variations seen in seismic tomography are likely to be related to lateral variations in temperature. Quantifying this relationship has proved difficult, in part because of the non-uniqueness of tomographic models (e.g. damping) and remaining uncertainties in key mineralogical properties. Because the magnitude of lateral variations is small, consideration of second-order effects such as attenuation and dispersion are important, if still ill-constrained experimentally, particularly at mantle pressures. Lateral variations in chemical composition almost certainly contribute as well, for example associated with depletion of the continental lithospheric mantle. In the deep mantle, the relationship between lateral variations in S- and P-wave velocities cannot be explained by lateral variations in temperature alone, although what other causes might be responsible is still a matter of debate.

Here we demonstrate another important contributor to lateral heterogeneity that has so far received little attention: that due to lateral variations in phase proportions and compositions (Anderson, 1987). We will argue that the contribution from phase transformations is reasonably well constrained experimentally, is comparable in magnitude to that of temperature alone in a monophase aggregate, and should be included in future analyses of three-dimensional structure. We first outline the thermodynamic theory and illustrate the effect of phase transformations with examples. We then explore the influence of phase transformations on the temperature variation of velocity and density in a realistic mantle composition. Finally we draw some conclusions regarding the likely importance of phase transformations in the interpretation of mantle structure.

2. Theory

Consider the seismic wave velocity in the vicinity of a phase transformation (Fig. 1). Because the mantle is a multi-component system, phase transformations generally occur over a finite depth interval, ΔP . Assume that the velocity contrast between the two phases is ΔV . It is generally assumed that the passage of the seismic wave is sufficiently rapid and the stresses generated sufficiently small, that no phase transformation is induced. In this case, the velocity increases monotonically with increasing depth across the phase transformation interval. The details of the shape of the transition, i.e. whether the velocity depends linearly or non-linearly on depth within the phase transformation interval (Stixrude, 1997) are not important for the present argument.

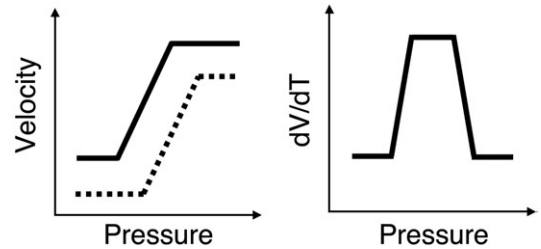


Fig. 1. Schematic illustration of (left) the seismic wave velocity in the vicinity of a phase transformation in a colder (solid) and hotter (dashed) portion of the mantle and (right) the temperature derivative of the velocity.

Assume for purposes of illustration that the phase transformation has a positive Clapeyron slope. The Clapeyron slope is not uniquely defined for multi-component phase transformations. For the purposes of illustration we may take the effective Clapeyron slope to be, for example, $\Gamma = (dP_{1/2}/dT)_{\text{eq}}$, where $P_{1/2}$ is the pressure at temperature T at which the phase transformation is half completed.

Now consider the same depth interval but at a different geographic location where the temperature is greater by δT (Fig. 1). The difference in velocity between colder and hotter mantle at the same depth represents the lateral variation in the velocity. The hotter mantle differs in two ways. First, the velocity is generally lower everywhere, in accord with the experimental observation that the velocity decreases with increasing temperature. Second, the phase transformation occurs at a greater depth. The difference in velocity is relatively small above and below the phase transformation interval and is governed by the temperature dependence of the velocity in the low and high-pressure assemblages, respectively. Within the phase transformation interval, the difference in velocity is much greater and is a function of the difference in velocity between the two transforming phases. Because the difference in velocity between phases is generally much larger than the influence of temperature on the velocity of a single phase, the contribution from phase transformations can be large.

Formally, we may write

$$\left(\frac{\partial \ln X}{\partial T}\right)_P = \left(\frac{\partial \ln X}{\partial T}\right)_{P, \vec{n}} + \left(\frac{\partial \ln X}{\partial \vec{n}}\right)_{P, T} \left(\frac{\partial \vec{n}}{\partial T}\right)_P \quad (1)$$

for the variation of the velocity or density with lateral variations in temperature where X is some physical property of the assemblage, such as the longitudinal, shear, or bulk sound velocity or the density, and \vec{n} is the vector specifying the amounts of all end-member species of all phases. The first term on the right hand

side may be called the isomorphic part: the derivative is taken at constant amounts and compositions of all coexisting phases. The second term may be called the metamorphic part and accounts for the variations in phase proportions (and compositions) with temperature.

The magnitude of the second term on the right hand side may be estimated

$$f\Gamma \frac{\Delta \ln V}{\Delta P} \quad (2)$$

where $\Delta \ln V$ is the relative difference in velocity between the two transforming phases, and f is the volume fraction of transforming phases. For example, in the case of the olivine to wadsleyite transition in a typical mantle composition, $f \sim 0.6$, $\Gamma \sim 4$ MPa/K, $\Delta \ln V_S \sim 9\%$, and $\Delta P \sim 0.5$ GPa (Bass, 1995; Katsura et al., 2004). These values yield a metamorphic contribution $-40 \times 10^{-5} \text{ K}^{-1}$, which is much larger than the influence of temperature on the velocity of either olivine or wadsleyite, for which $(d \ln V_S / dT)_n = -8.6 \times 10 \text{ K}$, and $-7.8 \times 10 \text{ K}$, respectively, in the elastic limit. For phase transformations with a negative Clapeyron slope, such as the ringwoodite = perovskite + periclase transition, the temperature derivative of the velocity will be positive within the phase transition interval, that is an increase in temperature will increase the velocity as more of the high-pressure assemblage is formed.

The variation of velocity with temperature is non-linear in the vicinity of phase transformations. This may be seen from Eqs. (1) (2) which show that in the vicinity of a first order transformation ($\Delta P = 0$), the metamorphic term diverges. More generally, and for a finite variation in temperature, δT , such that

$$\Gamma \delta T > \Delta P \quad (3)$$

the metamorphic term becomes

$$\frac{\Delta \ln V}{\delta T} \quad (4)$$

over a depth interval $\Gamma \delta T$. In the mantle, finite variations in temperature may induce additional phase transformations and stabilize new phase assemblages, further contributing to the non-linear dependence of velocity on temperature.

For transformations that occur over a narrow depth interval, such as the olivine to wadsleyite transition, the influence on lateral heterogeneity may alternatively be described in terms of the topography on the phase boundary. This description is sensible when the pressure interval over which the transition occurs is small compared with the topography on the phase boundary

due to lateral variations in temperature, i.e. when Eq. (3) is satisfied with δT the typical magnitude of lateral temperature variations in the mantle. This condition is satisfied for the olivine to wadsleyite transition: assuming $\delta T \sim 500$ K, the topography is 2 GPa or 56 km, much greater than the width of the transformation interval (0.3 GPa or 8 km), but not for example, by the orthopyroxene to garnet transition, for which $\Delta P \sim 11$ GPa.

3. Method

In order to investigate the likely effects of phase transformations on laterally varying structure in a realistic mantle composition, we use the method described in detail in our previous publications (Stixrude and Lithgow-Bertelloni, 2005a,b). Briefly, this is a thermodynamically self-consistent method, based on the concept of fundamental thermodynamic relations, that captures phase equilibria and physical properties, including the full elastic constant tensor, self-consistently. The form of the fundamental relation for the end-member species is based on Eulerian finite strain theory, and a Debye model of the vibrational density of states with the volume dependence of the characteristic frequency described by an Eulerian finite strain expansion. Activities are given by either ideal or symmetric regular solution models. The elastic moduli of the assemblage are computed as Voigt–Reuss–Hill averages of the constituent minerals. We use the same method to compute self-consistent adiabatic temperature profiles.

As in our previous work, we restrict ourselves to the five component system $\text{SiO}_2\text{--MgO--FeO--Al}_2\text{O}_3\text{--CaO}$, for which experimental data are most abundant. Some consequences of neglecting less abundant components, such as Na_2O are discussed below. We consider the following phases: anorthite (plg), spinel (sp), orthopyroxene (opx), clinopyroxene (cpx), high-pressure Mg-rich clinopyroxene (hpcpx), garnet (gt), olivine (ol), wadsleyite (wa), ringwoodite (ri), akimotoite (ak), perovskite (pv), CaSiO_3 perovskite (capv), and ferropericlase (fp), and stishovite (st).

The end-member species and the values of the parameters that describe their thermodynamics are specified in the supplementary material. These values are updated from our previous work (Stixrude and Lithgow-Bertelloni, 2005a,b) in the following ways. We have updated the parameters of several end-member phases based on more recent experimental data. For example, in situ measurements of the elastic wave velocities of high-pressure Mg-rich clinopyroxene (Kung et al., 2005). We have determined values of the reference free energy and

Debye temperature of the end-member species of higher pressure phases than those considered in (Stixrude and Lithgow-Bertelloni, 2005b), including ringwoodite, akimotoite, perovskite, and ferropericlasite.

We assume a composition thought to be representative of the source of mid-ocean ridge basalts and similar to many previous models of mantle composition including pyrolite: the depleted MORB mantle (DMM) of Workman and Hart (Workman and Hart, 2005). We compute properties along an adiabat with a potential temperature of 1600 K. Chemical equilibrium is assumed: at each pressure and temperature, the equilibrium phase assemblage, including phase proportions and chemical compositions is determined via a singular-value decomposition method that permits efficient application of the constant bulk composition constraint. The complete temperature derivative is computed by central finite difference: at each pressure (depth), a small finite temperature increment is applied and the equilibrium phase assemblage and its physical properties recomputed. For comparison we also compute analytically the isomorph part of the temperature derivative via

$$\left(\frac{\partial \ln V}{\partial T}\right)_{P,n} = \frac{1}{2} \left[\frac{1}{M} \left(\frac{\partial M}{\partial T}\right)_{P,n} + \alpha \right]$$

$$\left(\frac{\partial M}{\partial T}\right)_{P,n} = \left(\frac{\partial M}{\partial T}\right)_{\rho,n} - \alpha K_T \left(\frac{\partial M}{\partial P}\right)_{T,n}$$

$$= -\eta \rho C_\rho - \alpha K_T M' \quad (5)$$

where M is the elastic modulus, $V = \sqrt{M/\rho}$, α is the isomorph thermal expansivity, η is the shear part of the strain derivative of the Grüneisen parameter, C_ρ is the isochoric heat capacity, K_T is the isothermal bulk modulus, and M' is the isothermal pressure derivative of M .

We include the influence of anelasticity on the temperature derivative (Karato, 1993). Following Stixrude and Lithgow-Bertelloni (2005b), we approximate the quality factor

$$Q(z) = Q_{00}(z) \exp \left[\frac{\alpha E^*}{R} \left(\frac{1}{T(z)} - \frac{1}{T_R(z)} \right) \right] \quad (6)$$

where $Q_{00}(z)$ is the radial part of the seismological quality model QR19 (Romanowicz, 1995), T is the temperature, T_R is the temperature along the 1600 K adiabat, and values of the activation energy $E^* = 424 \text{ kJ mol}^{-1} \text{ K}^{-1}$ and frequency exponent, $\alpha = 0.26$, are from Jackson et al. (2002). The activation energy is assumed to be independent of pressure in the absence of

experimental data at elevated pressure. Allowing E^* to depend on pressure via the Weertman law, or a plausible finite value of the activation volume, has little influence on the results of our study.

4. Results

The computed phase assemblage along the reference adiabat is in good agreement with our previous results and many previous studies (Ita and Stixrude, 1992; Cammarano et al., 2003; Stixrude and Lithgow-Bertelloni, 2005b) (Fig. 2). As in our previous work, which extended to a depth of 500 km (Stixrude and Lithgow-Bertelloni, 2005b), the amount of cpx appears to be underestimated as compared with experiment and this is likely due to the neglect of the jadeite component of cpx in our study. The sequence of transformations at higher pressures also agrees with previous experimental results including the pressure and width of the wadsleyite to ringwoodite transition, the pressure at which CaSiO_3 perovskite first appears, the position of the ringwoodite to perovskite + ferropericlasite transition and the disappearance of garnet (Irfune, 1994). We find a small amount of akimotoite along the reference adiabat, which is consistent with previous experimental studies (Hirose, 2002). The self-consistent reference adiabat reflects the exchange of latent heat at phase boundaries (Verhoogen effect Verhoogen, 1965), including an increase in temperature at the olivine = wadsleyite and wadsleyite = ringwoodite transitions, and a decrease in temperature at the ringwoodite = perovskite + ferropericlasite transition.

The computed shear wave velocity along the reference adiabat agrees well with our previous result and other studies (Fig. 3). Over the depth range explored in our previous study, the velocity along the same geotherm differs by less than 0.03 km s^{-1} , due to updated values of

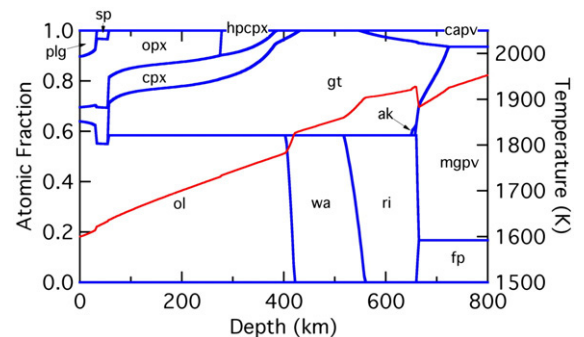


Fig. 2. Computed phase equilibria (blue) and self-consistent adiabat temperature profile assuming a potential temperature of 1600 K (red). (For interpretation of the references to colour in this figure legend, the reader is referred to the web version of this article.)

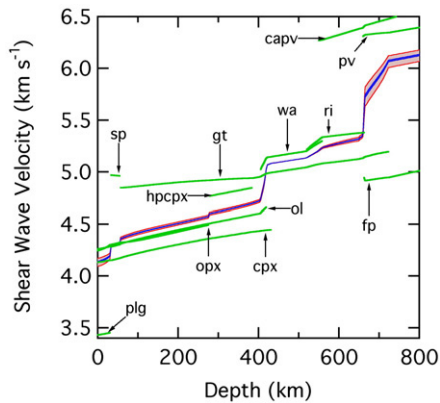


Fig. 3. Computed shear wave velocity of the individual minerals (green) plotted over their range of stability and that of the aggregate (blue). The red envelop shows the Reuss and Voigt bounds. (For interpretation of the references to colour in this figure legend, the reader is referred to the web version of this article.)

the relevant parameters as discussed in the Methods section and a slightly different assumed bulk composition. At greater depths, the velocity structure is very similar to that found in other studies, including the presence of a prominent 660 km discontinuity due to the ringwoodite=perovskite+ferropericalse transition, and a high gradient zone at greater depths due to the transition of garnet to perovskite (Stixrude, 1997; Weidner and Wang, 1998; Akaogi et al., 2002). Also present, as expected, is a high gradient zone due to the wa=ri and gt=capv transitions, and a small velocity discontinuity associated with the appearance of akimotoite. The latter feature is strongly dependent on temperature, with akimotoite becoming more

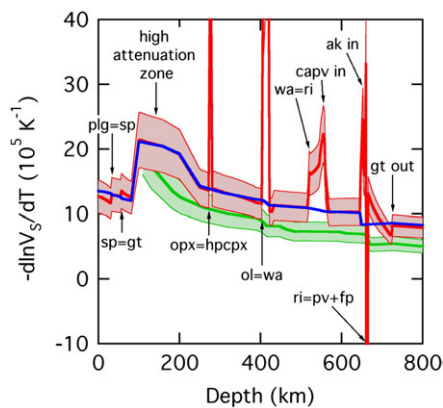


Fig. 4. Temperature derivative of the shear wave velocity along the 1600 K adiabat (red) and the isomorphous contribution (blue). The red envelope indicates nominal uncertainties. We compare with the results of Cammarano et al. (2003) (green). (For interpretation of the references to colour in this figure legend, the reader is referred to the web version of this article.)

abundant, at the expense of garnet, with decreasing temperature (Weidner and Wang, 1998). As in our previous study, the velocities of individual mineral phases reflect thermodynamic self-consistency between phase equilibria and physical properties. For example, within the olivine to wadsleyite transition interval, the velocity of both phases changes rapidly with depth due to the influence of iron partitioning among the transforming (ol,wa) and non-transforming (cpx, gt) phases. This partitioning influences the width and detailed shape of the transition and is important for understanding seismic reflectivity (Stixrude, 1997; Irifune and Isshiki, 1998).

The temperature derivative of the velocity along the 1600 K adiabat shows the important influence of phase transformations, as anticipated by our simple analysis (Fig. 4). The total temperature derivative has a value much larger than that of the isomorphous part in the vicinity of phase transformations. The difference may be more than a factor of four. For example, the total derivative within the ol=wa phase transition interval reaches a maximum value of $-55 \times 10^{-5} \text{ K}^{-1}$, and the metamorphic contribution is $-43 \times 10^{-5} \text{ K}^{-1}$, in good agreement with our approximate analysis above.

The metamorphic contribution to the temperature derivative is also apparent in the vicinity of other phase transformations along the reference adiabat, including the plg=sp, sp=gt, opx=hpcpx, wa=ri, ri=pv+fp transitions, and the appearance of akimotoite, and the dissolution of garnet into perovskite. As with the olivine to wadsleyite transition, the magnitude of the metamorphic contribution may exceed that of the isomorphous term, albeit not invariably. The magnitude and sign in all cases can be understood on the basis of the approximate relation Eq. (2).

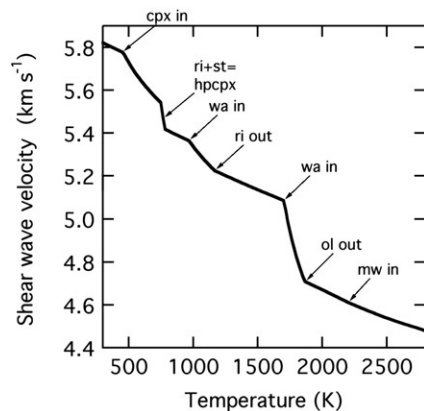


Fig. 5. Elastic part of the shear wave velocity versus temperature at 410 km depth (13.8 GPa).

We note that the isomorphic part of the temperature derivative decreases with increasing pressure as expected, and as found in previous studies that neglected the metamorphic part. Our values for the isomorphic contribution are somewhat larger than those of (Cammarrano et al., 2003). There are two reasons for this difference. Our thermodynamic model captures the non-linear dependence of the elastic part of the velocity on temperature as required by the third law, whereas Cammarano et al. (2003), and many other previous studies of the upper mantle and transition zone (Vacher et al., 1998; Goes et al., 2000), assume a linear dependence from ambient temperature to mantle temperatures. We have also made different assumptions regarding the attenuation structure, that are more closely linked to the actual attenuation structure of the mantle as revealed by seismological observations.

The temperature derivative of the velocity depends on the temperature itself, i.e. the variation of velocity with temperature is non-linear over the typical mantle temperature regime. The reason is that the phase equilibria change with variations in temperature over the mantle range. For example, at 410 km depth (Fig. 5) the velocity varies much more rapidly over the temperature interval of the olivine to wadsleyite transition than at greater or lesser temperatures. Other rapid changes in the velocity with temperature at 410 km depth occur at the wadsleyite to ringwoodite transition at temperatures typical of subducting slabs (~ 1000 K) and at the appearance of stishovite on cooling near 750 K.

We further illustrate the non-linear dependence of velocity on temperature by computing the velocity difference over a finite temperature interval δT , from a potential temperature of 1000 K, typical of subduction zones, to 1700 K, typical of upwelling plumes (Fig. 6). This differential quantity $\delta \ln V / \delta T$ represents the average temperature derivative over the mantle temperature regime. As anticipated the prominent peaks in the metamorphic term now have lesser magnitude ($\Delta \ln V / \delta T$) and are spread over a broader depth interval ($\sim T \delta T$). The metamorphic contributions to the differential are comparable to the isomorphic contributions and are significant over most of the upper 800 km. The peaks associated with the wa=ri, gt=capv, and the gt=ri+st transitions (the latter important at low temperature) overlap and occupy most of the depth interval of the transition zone, except for the upper and lower boundaries of this region where the metamorphic contributions of the olivine to wadsleyite and the ringwoodite to perovskite and periclase transition appear.

The metamorphic part of the thermal expansivity has an important influence on mantle dynamics (Richter,

1973; Schubert et al., 1975). The thermal expansivity shows many of the same features as the temperature derivative of the velocity (Fig. 7). In particular, the metamorphic contribution is large and important throughout much of the upper mantle and transition zone. The relationship to parameters appearing in the approximate forms of the conservation equations upon which mantle convection simulations are based (Christensen and Yuen, 1985) is

$$\Pi \frac{dY}{dp} = \frac{\alpha_{\text{met}}}{\alpha_{\text{iso}}} \quad (7)$$

where α_{met} and α_{iso} are the metamorphic and isomorphic parts of the thermal expansivity, respectively, Y is the proportion of the high-pressure phase, p is a non-dimensional pressure, and Π is the phase buoyancy parameter

$$\Pi = - \frac{\int_{\Delta P} \alpha_{\text{met}} dP}{\langle \rho \rangle \langle \alpha_{\text{iso}} \rangle g h} \quad (8)$$

where the denominator is the thermal buoyancy, the angle brackets denote an average over the entire mantle, and h is the depth of the mantle. The usual formulation of this term, which appears on the left hand side in Eq. (7) is problematic because many phase transformations are relevant and the intervals of transformation in some cases overlap. We also note that the ad hoc functional forms typically assumed for $Y(p)$, such as the hyperbolic tangent, differ significantly from the correct form demanded by the Lever rule (Stixrude, 1997). For these reasons, the reformulation of the phase buoyancy term on the right hand side of Eq. (7) with α_{met} and α_{iso} computed from the self-consistent thermodynamics of the multi-

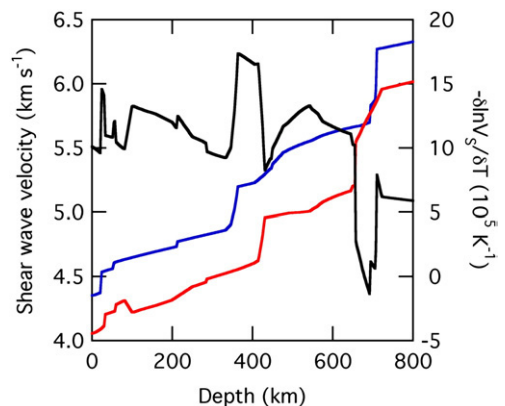


Fig. 6. Shear wave velocity along 1600 K (red) and 1000 K (blue) adiabats, and the relative difference $\delta \ln V_s / \delta T$ (black, right-hand axis). (For interpretation of the references to colour in this figure legend, the reader is referred to the web version of this article.)

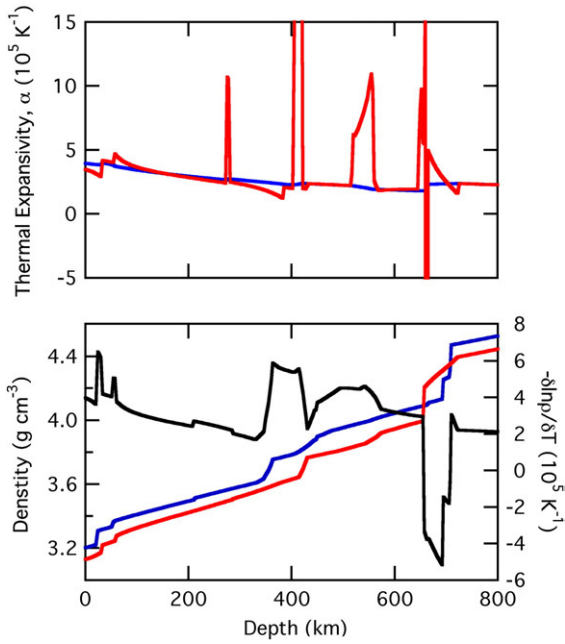


Fig. 7. (top) Thermal expansivity along the 1600 K adiabat (red) and the isomorph contribution (blue). (bottom) Density along 1600 K (red) and 1000 K (blue) adiabats, and the relative difference $\delta \ln \rho / \delta T$ (black, right-hand axis). (For interpretation of the references to colour in this figure legend, the reader is referred to the web version of this article.)

component system, is a more complete and accurate representation of the relevant physics. For comparison to existing studies of mantle convection, we have computed the value of Π from our results for α_{met} and Eq. (8) for the three prominent sets of peaks in α_{mc} near 410, 520, and 660 km depth. Assuming typical values $\langle \rho \rangle =$

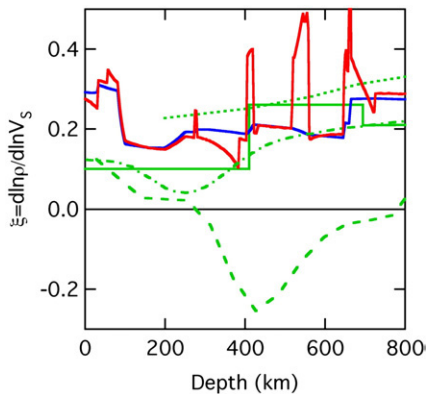


Fig. 8. Relative variations of density and shear wave velocity ξ (red) and the isomorph contribution to ξ (blue) compared with the results of: (short-dashed green) Karato (1993), (solid green) Forte et al. (1994), (long-dashed green) Ishii and Tromp (2001) and (dash-dot green) Forte and Mitrovica (2001). (For interpretation of the references to colour in this figure legend, the reader is referred to the web version of this article.)

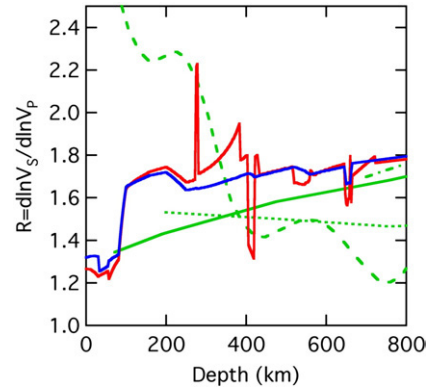


Fig. 9. Relative variations of shear and longitudinal wave velocity R (red) and the isomorph contribution to R (blue) compared with the results of: (solid green) Bolton and Masters (2001) (short dashed green) Karato (1993) (long-dashed green) Ishii and Tromp (2001), and (dash-dot green) Robertson and Woodhouse (1996). (For interpretation of the references to colour in this figure legend, the reader is referred to the web version of this article.)

3000 kg m^{-3} , $\langle \alpha \rangle = 3 \times 10^{-5} \text{ K}^{-1}$, $g = 10 \text{ m/s}^2$, and $h = 2890 \text{ km}$, we find $\Pi = 0.042$, 0.037 , and -0.072 for these three groups of transitions.

The relative magnitudes of lateral variations in shear and longitudinal wave velocities and density permit comparisons of seismological models to other geophysical observables such as the geoid. If lateral variations are assumed to be caused solely by lateral variations in temperature

$$\xi = \left(\frac{\partial \ln \rho}{\partial \ln T} \right)_p / \left(\frac{\partial \ln V_s}{\partial \ln T} \right)_p \quad (7)$$

$$R = \left(\frac{\partial \ln V_s}{\partial \ln T} \right)_p / \left(\frac{\partial \ln V_p}{\partial \ln T} \right)_p \quad (8)$$

where the derivatives are the total derivatives and must include the influence of phase transformations, as well as the isomorph contribution. Our results show considerable variation with depth due to the influence of phase transformations (Figs. 8 and 9). The metamorphic contribution to ξ is positive for most phase transitions, consistent with expectations based on Birch's law. The region near 350 km depth is an exception and shows a negative metamorphic contribution due to the pyroxene to garnet transition. Most previous analyses show less variation with depth as compared with our results. For example, the results of Forte et al. (1994) are based on inverting gravity observations. As these observations have limited depth resolution, one might expect the results of the inversion to show more gradual variations in depth. In fact the results of Forte et al. (1994) appear to

agree well with a depth-smoothed version of our results. A more recent and more elaborate inversion (Forte and Mitrovica, 2001), produces similar results in the upper 800 km, with ξ approximately 20% smaller in the transition zone. The results of Karato (1993) are based on experimental data, but did not consider the influence of phase transformations. The results of Ishii and Tromp (2001) are based on inversions of normal mode observations and free-air gravity. Their results are very different from ours, in particular they find a negative value of ξ in the upper mantle (anti-correlation of density and shear wave velocity). Since our results show a positive value of ξ everywhere, the result of Ishii and Tromp could only be explained by large lateral variations in bulk composition.

5. Discussion

The highly non-linear dependence of the velocity–temperature scaling with depth has important consequences for understanding the structure of the mantle (Fig. 10). In the vicinity of sharp phase transformations, the sensitivity of seismic wave velocities to temperature changes suddenly over a narrow range of depth. This means that the magnitude of lateral variations in either i) temperature or ii) seismic wave velocities must depend strongly on depth. For example, in the vicinity of 400 km depth, where the magnitude of $\ln V/dT$ is large, temperature anomalies must be dramatically subdued, or the size of seismic velocity anomalies must be much greater than those at slightly shallower or greater depths. The

latter seems most likely since sudden changes in thermal structure of the required size are not expected on dynamical grounds. For example, in a thermal model of a subducting slab (Sleep, 1973) the magnitude of lateral temperature variations decreases by less than 1% per 10 km increase in depth, as compared with factor of five change over the same depth range that would be required in the vicinity of the olivine to wadsleyite transition.

In contrast to these expectations, the amplitude of tomographic models varies smoothly with depth (Romanowicz, 2003). This may be due to the limited ability of tomographic studies to resolve rapid changes in mantle structure as a function of depth.

We construct a picture of velocity and temperature structure of the mantle that is consistent with geodynamic expectations and the finite spatial resolution of tomographic models (Fig. 10 bottom row). The amplitude of mantle thermal structure varies smoothly and gradually with depth. In this case, based on our results, the magnitude of lateral variations in velocity must vary rapidly with depth. It is just these rapid variations with depth that tomographic models are not likely to capture because they fall below the spatial resolution of the data upon which they are based.

The arguments of this section have important implications for the interpretation of tomographic models, particularly in the upper 1000 km, and possibly the bottom few hundred km, where phase transformations have a large influence on the structure. A naïve application of a velocity–temperature scaling derived from experiment is not likely to yield realistic results. If the influence of phase

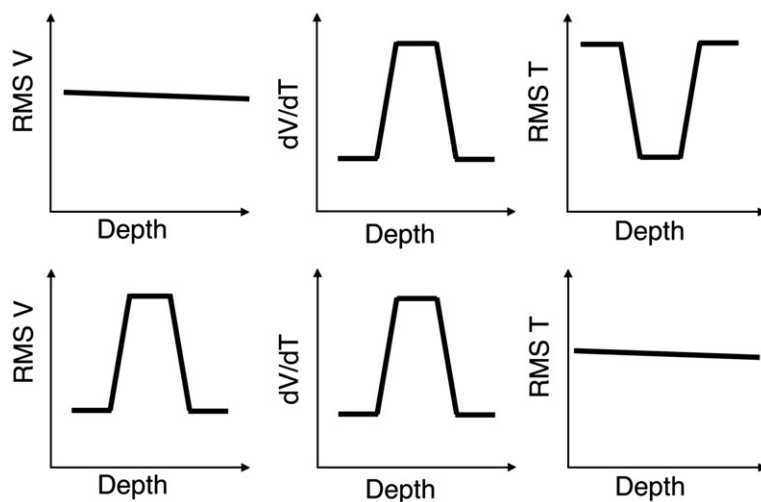


Fig. 10. Schematic illustrations of the consequences of smooth variations with depth of the amplitude of tomographic models (top row) versus smooth variations with depth of the amplitude of lateral temperature variations (bottom row). The right-most column shows the amplitude of lateral variations in velocity with depth, the central column a schematic representation of the temperature derivative of the velocity in the vicinity of a phase transformation, and the left-most column, the amplitude of lateral variations in temperature with depth.

transformations is ignored, as they are in several previous studies (Goes et al., 2000; Cammarano et al., 2003), the physics embodied in the scaling is incomplete and not representative of the multi-phase mantle. If the influence of phase transformations is included, one finds unrealistically rapid variations of the temperature structure with depth.

The difficulty of interpreting tomographic models in terms of mantle thermal structure illustrates the limited ability of tomographic models to capture the essential features of the metamorphic contribution. Tomographic models might be augmented by an explicit representation of laterally varying discontinuity structure using data that are particularly sensitive to boundary topography (Masters et al., 1996). An alternative approach would be based more closely on the actual observations, i.e. travel times and normal mode frequencies. For example, seismological observables could be computed from a mineralogical model of the mantle, with lateral variations in velocity determined by the scalings found here, and compared with observations directly.

Geodynamical models that explore the influence of phase transformations on mantle convection typically focus on the transitions responsible for the 410 and 660 km seismic discontinuities: $ol=wa$, and $ri=pv+fp$. Our results indicate that a series of transitions near 520 km depth, including $wa=ri$, $gt=capv$, and $gt=ri+st$, may be equally important. The integrated phase buoyancy parameter for these transitions is nearly equal in magnitude to that of the $ol=wa$ transition and should be included in future studies. We find that the combined buoyancy of the $ol=wa$ and ~ 520 km transitions is almost exactly balanced by that of the perovskite forming transitions near 660 km depth.

We have not considered partial melt in our analysis. Partial melt has an important influence on seismic wave velocities in the immediate vicinity of mid-ocean ridges (Webb and Forsyth, 1998), although it appears to be absent from most of the low velocity zone (Stixrude and Lithgow-Bertelloni, 2005b), and possibly at the 410 km discontinuity (Revenaugh and Sipkin, 1994), and at the base of the mantle (ultra-low velocity zone) (Williams and Garnero, 1996; Revenaugh and Meyer, 1997). Incorporation of melt in our analysis will be the subject of future work and lies beyond the scope of our present study for at least two reasons: 1) the influence of melt on seismic wave velocity depends critically on the texture of the melt, which is poorly constrained, i.e. the Voigt and Reuss bounds on the velocity of partial melts are widely separated 2) the presence of melt is often associated with a change in chemical composition, for example, depletion of the oceanic lithosphere, or the addition of

water as has been proposed for the thermodynamic stabilization of melts at the 410 km discontinuity (Revenaugh and Sipkin, 1994). Another useful future direction would be to incorporate into our analysis water as a component and the large number of hydrous and nominally anhydrous phases in which it might exist (Komabayashi, 2006). For the range of water contents typically considered to exist in the mantle, the influence of water is likely to be largest in 1) stabilizing new phases, such as melt, or hydrous mineral phases, particularly at slab-like temperatures and 2) enhancing attenuation, although there are at present essentially no experimental data that allow us to quantify this effect.

6. Conclusions

There are three potential causes of laterally varying structure: lateral variations in temperature, chemical composition, and phase. The first two of these have received most attention. Lateral variations in phase are likely to be important as well, particularly in the upper 800 km of the mantle, where phase transformations are ubiquitous, and possibly in the lowermost few hundred km of the mantle. The contributions of phase transformations to the scaling of velocity to temperature or density are easily understood and reasonably well constrained by extant experimental information. The metamorphic contribution to these scaling relationships should be included in future studies relating seismic structure of the mantle to thermal structure or the gravitational field. Some care must be taken because of the mis-match between the rapid variations in depth of the scalings and the relatively low spatial resolution of tomographic models. Interpretation of tomographic models in terms of mantle temperature structure is therefore frustrated to some extent by the fact that comparisons are not to seismological observations, but to seismological models, which are non-unique. One might envision using our models in two ways to overcome this limitation: 1) testing directly against seismological data by computing seismological observables from the mineralogical model. Computation of travel times and normal mode frequencies from a mineralogical model including the influence of phase transformations on radial and laterally varying structure is in principle straightforward. 2) Using mineralogical models as a starting point for exploring the range of seismological models that match the data equally well, i.e. the null space of the inverse problem. The influence of phase transformations on laterally varying structure is especially strong in the upper mantle and transition zone. Approaches such as these may be essential for

unraveling the relative contributions of lateral variations in temperature, bulk composition and phase to the three-dimensional structure of these regions.

Our results also show the importance of considering the complete multi-phase thermodynamics in models of mantle convection. The influence of phase transformations is not adequately captured by approximate treatments of the 410 and 660 km discontinuities alone. The 520 km discontinuity appears to be important as well. Moreover, the influence of temperature on buoyancy is expected to be non-linear, with phase assemblages changing significantly over wide depth ranges in the upper mantle and transition zone. One might envision coupling a mantle convection model to a mineralogical–thermodynamical model such as ours, possibly by means of a lookup table of physical properties, including density and enthalpy, as a function of depth and temperature.

Acknowledgements

We thank Alex Forte and an anonymous reviewer for thoughtful comments that improved the manuscript. This work supported by the U.S. National Science Foundation under grants EAR-0635815 and EAR-0456112.

Appendix A. Supplementary data

Supplementary data associated with this article can be found, in the online version, at [doi:10.1016/j.epsl.2007.08.027](https://doi.org/10.1016/j.epsl.2007.08.027).

References

- Akaogi, M., Tanaka, A., Ito, E., 2002. Garnet–ilmenite–perovskite transitions in the system $\text{Mg}_4\text{Si}_4\text{O}_{12}$ – $\text{Mg}_3\text{Al}_2\text{Si}_3\text{O}_{12}$ at high pressures and high temperatures: phase equilibria, calorimetry and implications for mantle structure. *Phys. Earth Planet. Inter.* 132, 303–324.
- Anderson, D.L., 1987. Thermally induced phase-changes, lateral heterogeneity of the mantle, continental roots, and deep slab anomalies. *J. Geophys. Res., Solid Earth Planets* 92, 13968–13980.
- Bass, J.D., 1995. Elasticity of minerals, glasses, and melts. In: Ahrens, T.J. (Ed.), *Mineral Physics and Crystallography: A Handbook of Physical Constants*. American Geophysical Union, Washington, DC, pp. 45–63.
- Bolton, H., Masters, G., 2001. Travel times of P and S from the global digital seismic networks: implications for the relative variation of P and S velocity in the mantle. *J. Geophys. Res., Solid Earth* 106, 13527–13540.
- Cammarano, F., Goes, S., Vacher, P., Giardini, D., 2003. Inferring upper-mantle temperatures from seismic velocities. *Phys. Earth Planet. Inter.* 138, 197–222.
- Christensen, U.R., Yuen, D.A., 1985. Layered convection induced by phase transitions. *J. Geophys. Res.* 90, 10291–10300.
- Forte, A.M., Mitrovica, J.X., 2001. Deep-mantle high-viscosity flow and thermochemical structure inferred from seismic and geodynamic data. *Nature* 410, 1049–1056.
- Forte, A.M., Woodward, R.L., Dziewonski, A.M., 1994. Joint inversions of seismic and geodynamic data for models of 3-dimensional mantle heterogeneity. *J. Geophys. Res., Solid Earth* 99, 21857–21877.
- Goes, S., Govers, R., Vacher, P., 2000. Shallow mantle temperatures under Europe from P and S wave tomography. *J. Geophys. Res., Solid Earth* 105, 11153–11169.
- Hirose, K., 2002. Phase transitions in pyrolitic mantle around 670-km depth: implications for upwelling of plumes from the lower mantle. *J. Geophys. Res., Solid Earth* 107 (B4), 2078, [doi:10.1029/2001JB000597](https://doi.org/10.1029/2001JB000597).
- Irifune, T., 1994. Absence of an aluminous phase in the upper part of the Earth's Lower Mantle. *Nature* 370, 131–133.
- Irifune, T., Isshiki, M., 1998. Iron partitioning in a pyrolite mantle and the nature of the 410-km seismic discontinuity. *Nature* 392, 702–705.
- Ishii, M., Tromp, J., 2001. Even-degree lateral variations in the Earth's mantle constrained by free oscillations and the free-air gravity anomaly. *Geophys. J. Int.* 145, 77–96.
- Ita, J., Stixrude, L., 1992. Petrology, elasticity, and composition of the mantle transition zone. *J. Geophys. Res., Solid Earth* 97, 6849–6866.
- Jackson, I., Gerald, J.D.F., Faul, U.H., Tan, B.H., 2002. Grain-size-sensitive seismic wave attenuation in polycrystalline olivine. *J. Geophys. Res., Solid Earth* 107 (B12), 2360, [doi:10.1029/2001JB001225](https://doi.org/10.1029/2001JB001225).
- Katsura, T., Yamada, H., Nishikawa, O., Song, M.S., Kubo, A., Shinmei, T., Yokoshi, S., Aizawa, Y., Yoshino, T., Walter, M.J., Ito, E., Funakoshi, K., 2004. Olivine–wadsleyite transition in the system $(\text{Mg,Fe})_2\text{SiO}_4$. *J. Geophys. Res., Solid Earth* 109, B02209, [doi:10.1029/2003JB002438](https://doi.org/10.1029/2003JB002438).
- Karato, S., 1993. Importance of anelasticity in the interpretation of seismic tomography. *Geophys. Res. Lett.* 20, 1623–1626.
- Komabayashi, T., 2006. Phase relations of hydrous peridotite: implications for water circulation in the Earth's mantle. In: Jacobsen, S.D., van der Lee, S. (Eds.), *Earth's Deep Water cycle*. American Geophysical Union, Washington, DC, pp. 29–44.
- Kung, J., Li, B.S., Uchida, T., Wang, Y.B., 2005. In-situ elasticity measurement for the unquenchable high-pressure clinopyroxene phase: implication for the upper mantle. *Geophys. Res. Lett.* 32, L01307, [doi:10.1029/2004GL021661](https://doi.org/10.1029/2004GL021661).
- Masters, G., Johnson, S., Laske, G., Bolton, H., 1996. A shear-velocity model of the mantle. *Philos. Trans. R. Soc. Lond. Ser. A: Math. Phys. Eng. Sci.* 354, 1385–1410.
- Revenaugh, J., Meyer, R., 1997. Seismic evidence of partial melt within a possibly ubiquitous low-velocity layer at the base of the mantle, 277, 670–673.
- Revenaugh, J., Sipkin, S.A., 1994. Seismic evidence for silicate melt atop the 410 km mantle discontinuity. *Nature* 369, 474–476.
- Richter, F.M., 1973. Finite-amplitude convection through a phase boundary. *Geophys. J. R. Astron. Soc.* 35, 265–276.
- Robertson, G.S., Woodhouse, J.H., 1996. Ratio of relative S to P velocity heterogeneity in the lower mantle. *J. Geophys. Res.* 101, 20,041–20,052.
- Romanowicz, B., 1995. A global tomographic model of shear attenuation in the upper-mantle. *J. Geophys. Res., Solid Earth* 100, 12375–12394.
- Romanowicz, B., 2003. Global mantle tomography: progress status in the past 10 years. *Annu. Rev. Earth Planet. Sci.* 31, 303–328.
- Schubert, G., Yuen, D.A., Turcotte, D.L., 1975. Role of phase-transitions in a dynamic mantle. *Geophys. J. R. Astron. Soc.* 42, 705–735.

- Sleep, N.H., 1973. Teleseismic P-wave transmission through slabs. *Bull. Seismol. Soc. Am.* 63, 1349–1373.
- Stixrude, L., 1997. Structure and sharpness of phase transitions and mantle discontinuities. *J. Geophys. Res., Solid Earth* 102, 14835–14852.
- Stixrude, L., Lithgow-Bertelloni, C., 2005a. Thermodynamics of mantle minerals — I. Physical properties. *Geophys. J. Int.* 162, 610–632.
- Stixrude, L., Lithgow-Bertelloni, C., 2005b. Mineralogy and elasticity of the oceanic upper mantle: origin of the low-velocity zone. *J. Geophys. Res., Solid Earth* 110, B03204, doi:10.1029/2004JB002965.
- Vacher, P., Mocquet, A., Sotin, C., 1998. Computation of seismic profiles from mineral physics: the importance of the non-olivine components for explaining the 660 km depth discontinuity. *Phys. Earth Planet. Inter.* 106, 275–298.
- Verhoogen, J., 1965. Physics of convection currents in Earth's mantle. 22. phase Changes and convection in Earth's mantle. *Philos. Trans. R. Soc. Lond. Ser. A: Math. Phys. Sci.* 258, 276–283.
- Webb, S.C., Forsyth, D.W., 1998. Structure of the upper mantle under the EPR from waveform inversion of regional events. *Science* 280, 1227–1229.
- Weidner, D.J., Wang, Y.B., 1998. Chemical- and clapeyron-induced buoyancy at the 660 km discontinuity. *J. Geophys. Res., Solid Earth* 103, 7431–7441.
- Williams, Q., Garnero, E.J., 1996. Seismic evidence for partial melt at the base of Earth's mantle. *Science* 273, 1528.
- Workman, R.K., Hart, S.R., 2005. Major and trace element composition of the depleted MORB mantle (DMM). *Earth Planet. Sci. Lett.* 231, 53–72.

Supplementary Material: Influence of phase transformations on lateral heterogeneity and dynamics in Earth's mantle

Lars Stixrude and Carolina Lithgow-Bertelloni
Department of Geological Sciences
University of Michigan
Ann Arbor, MI 48109-1005

As discussed in the main text, our work is based on a semi-empirical thermodynamic model, which allows self-consistent computation of all isotropic physical properties, phase equilibria, and shear elasticity over the mantle regime. The values of the parameters of the thermodynamic model used in this study are given in Supplementary Table 1. These are: the values of the Helmholtz free energy, F_0 , volume, V_0 , bulk modulus, K_0 , pressure derivative of the bulk modulus, K_0' , Debye temperature, θ_0 , Grüneisen parameter, γ_0 , logarithmic volume derivative of the Grüneisen parameter, q_0 , shear modulus, G_0 , pressure derivative of the shear modulus, G_0' , shear part of the strain derivative of the Grüneisen parameter, η_{s0} , and the regular solution parameter W , at ambient conditions for each of the 31 end-member species considered here. Values of the parameters have been updated to take account of more recent experimental data as indicated in section 3 of the main text.

Supplementary References

- [1] J.R. Smyth, T.C. McCormick, Crystallographic data for minerals, in: T.J. Ahrens, (Ed), Mineral Physics and Crystallography: A Handbook of Physical Constants, American Geophysical Union, Washington, DC, 1995, pp. 1-17.
- [2] J.D. Bass, Elasticity of minerals, glasses, and melts, in: T.J. Ahrens, (Ed), Mineral Physics and Crystallography: A Handbook of Physical Constants, American Geophysical Union, Washington, DC, 1995, pp. 45-63.
- [3] R.J. Angel, High-Pressure Structure of Anorthite, *American Mineralogist* 73(1988) 1114-1119.
- [4] R.A. Robie, B.S. Hemingway, Thermodynamic Properties of Minerals and Related Substances at 298.15 K and 1 Bar (10^5 Pascals) Pressure and at Higher Temperature, U. S. Geological Survey, Washington, DC, 1995, 461 pp.
- [5] Y. Fei, Thermal Expansion, in: T.J. Ahrens, (Ed), Mineral Physics and Crystallography: A Handbook of Physical Constants, American Geophysical Union, Washington, DC, 1995, pp. 29-44.
- [6] A. Yoneda, Pressure Derivatives of Elastic-Constants of Single-Crystal MgO and MgAl₂O₄, *Journal of Physics of the Earth* 38(1990) 19-55.
- [7] G. Fiquet, P. Richet, G. Montagnac, High-temperature thermal expansion of lime, periclase, corundum and spinel, *Physics and Chemistry of Minerals* 27(1999) 103-111.
- [8] O.L. Anderson, D.G. Isaak, Elastic constants of mantle minerals at high temperature, in: T.J. Ahrens, (Ed), Mineral Physics and Crystallography: A Handbook of Physical Constants, American Geophysical Union, Washington, DC, 1995, pp. 64-97.
- [9] L.M. Anovitz, E.J. Essene, G.W. Metz, S.R. Bohlen, E.F. Westrum, B.S. Hemingway, Heat-Capacity and Phase-Equilibria of Almandine, Fe₃Al₂Si₃O₁₂, *Geochimica Et Cosmochimica Acta* 57(1993) 4191-4204.
- [10] R.J. Harrison, S.A.T. Redfern, H.S.C. O'Neill, The temperature dependence of the cation distribution in synthetic hercynite (FeAl₂O₄) from in-situ neutron structure refinements, *American Mineralogist* 83(1998) 1092-1099.
- [11] C.S. Zha, T.S. Duffy, R.T. Downs, H.K. Mao, R.J. Hemley, Sound velocity and elasticity of single-crystal forsterite to 16 GPa, *Journal of Geophysical Research-Solid Earth* 101(1996) 17535-17545.
- [12] R.A. Robie, B.S. Hemingway, H. Takei, Heat-Capacities and Entropies of Mg₂SiO₄, Mn₂SiO₄, and Co₂SiO₄ between 5-K and 380-K, *American Mineralogist* 67(1982) 470-482.
- [13] M.A. Bouhifd, D. Andrault, G. Fiquet, P. Richet, Thermal expansion of forsterite up to the melting point, *Geophysical Research Letters* 23(1996) 1143-1146.
- [14] C.S. Zha, T.S. Duffy, R.T. Downs, H.K. Mao, R.J. Hemley, Brillouin scattering and X-ray diffraction of San Carlos olivine: direct pressure determination to 32 GPa, *Earth and Planetary Science Letters* 159(1998) 25-33.
- [15] E. Knittle, Static compression measurements of equations of state, in: T.J. Ahrens, (Ed), Mineral Physics and Crystallography: A Handbook of Physical Constants, American Geophysical Union, Washington, DC, 1995, pp. 98-142.

- [16] S.V. Sinogeikin, T. Katsura, J.D. Bass, Sound velocities and elastic properties of Fe-bearing wadsleyite and ringwoodite, *Journal of Geophysical Research-Solid Earth* 103(1998) 20819-20825.
- [17] C.S. Zha, T.S. Duffy, H.K. Mao, R.T. Downs, R.J. Hemley, D.J. Weidner, Single-crystal elasticity of beta-Mg₂SiO₄ to the pressure of the 410 km seismic discontinuity in the Earth's mantle, *Earth And Planetary Science Letters* 147(1997) E9-E15.
- [18] Y.W. Fei, H.K. Mao, J.F. Shu, G. Parthasarathy, W.A. Bassett, J.D. Ko, Simultaneous High-P, High-T X-Ray-Diffraction Study of Beta-(Mg,Fe)₂SiO₄ to 26-Gpa and 900-K, *Journal of Geophysical Research-Solid Earth* 97(1992) 4489-4495.
- [19] B.S. Li, R.C. Liebermann, D.J. Weidner, P-V-Vp-Vs-T measurements on wadsleyite to 7 GPa and 873 K: Implications for the 410-km seismic discontinuity, *Journal of Geophysical Research-Solid Earth* 106(2001) 30579-30591.
- [20] R. Jeanloz, A.B. Thompson, Phase transitions and mantle discontinuities, *Reviews of Geophysics* 21(1983) 51-74.
- [21] S.V. Sinogeikin, J.D. Bass, T. Katsura, Single-crystal elasticity of gamma-(Mg_{0.91}Fe_{0.09})₂SiO₄ to high pressures and to high temperatures, *Geophysical Research Letters* 28(2001) 4335-4338.
- [22] H.K. Mao, T. Takahashi, W.A. Bassett, J.S. Weaver, Effect of Pressure and Temperature on Molar Volumes of Wustite and of 3 (Fe Mg)₂SiO₄ Spinel Solid Solutions, *Journal of Geophysical Research* 74(1969) 1061-1069.
- [23] J.M. Jackson, S.V. Sinogeikin, J.D. Bass, Elasticity of MgSiO₃ orthoenstatite, *American Mineralogist* 84(1999) 677-680.
- [24] L.M. Flesch, B.S. Li, R.C. Liebermann, Sound velocities of polycrystalline MgSiO₃-orthopyroxene to 10 GPa at room temperature, *American Mineralogist* 83(1998) 444-450.
- [25] L. Thieblot, C. Tequi, P. Richet, High-temperature heat capacity of grossular (Ca₃Al₂Si₃O₁₂), enstatite (MgSiO₃), and titanite (CaTiSiO₅), *American Mineralogist* 84(1999) 848-855.
- [26] K.M. Krupka, R.A. Robie, B.S. Hemingway, D.M. Kerrick, J. Ito, Low-Temperature Heat-Capacities and Derived Thermodynamic Properties of Anthophyllite, Diopside, Enstatite, Bronzite, and Wollastonite, *American Mineralogist* 70(1985) 249-260.
- [27] J.M. Jackson, J.W. Palko, D. Andrault, S.V. Sinogeikin, D.L. Lakshtanov, J.Y. Wang, J.D. Bass, C.S. Zha, Thermal expansion of natural orthoenstatite to 1473 K, *European Journal of Mineralogy* 15(2003) 469-473.
- [28] Y.S. Zhao, D. Schiferl, T.J. Shankland, A High P-T Single-Crystal X-Ray-Diffraction Study of Thermoelasticity of MgSiO₃ Orthoenstatite, *Physics and Chemistry of Minerals* 22(1995) 393-398.
- [29] A.L. Frisillo, G.R. Barsch, Measurement of Single-Crystal Elastic-Constants of Bronzite as a Function of Pressure and Temperature, *Journal of Geophysical Research* 77(1972) 6360-6384.

- [30] D.A. HughJones, R.J. Angel, Effect of Ca²⁺ and Fe²⁺ on the equation of state of MgSiO₃ orthopyroxene, *Journal of Geophysical Research-Solid Earth* 102(1997) 12333-12340.
- [31] D. HughJones, Thermal expansion of MgSiO₃ and FeSiO₃ ortho- and clinopyroxenes, *American Mineralogist* 82(1997) 689-696.
- [32] B.J. Skinner, F.R. Boyd, Aluminous enstatites, *Carnegie Institution of Washington Yearbook* 63(1964) 163-165.
- [33] L. Levien, C.T. Prewitt, High-Pressure Structural Study of Diopside, *American Mineralogist* 66(1981) 315-323.
- [34] Y. Zhao, R.B.V. Dreele, J. Zhang, D.J. Weidner, Thermoelastic equation of state of monoclinic pyroxene: CaMgSi₂O₆, *Rev. High. Press. Sci. Tech.* 7(1998) 25-27.
- [35] H.T. Haselton, R.A. Robie, B.S. Hemingway, Heat-Capacities of Synthetic Hedenbergite, Ferrobustamite, and CaFeSi₂O₆ Glass, *Geochimica Et Cosmochimica Acta* 51(1987) 2211-2217.
- [36] M. Tribaudino, M. Prencipe, F. Nestola, M. Hanfland, A P21/c-C2/c high-pressure phase transition in Ca_{0.5}Mg_{1.5}Si₂O₆ clinopyroxene, *American Mineralogist* 86(2001) 807-813.
- [37] T. Shinmei, N. Tomioka, K. Fujino, K. Kuroda, T. Irifune, In situ X-ray diffraction study of enstatite up to 12 GPa and 1473 K and equations of state, *American Mineralogist* 84(1999) 1588-1594.
- [38] D. HughJones, T. Sharp, R. Angel, A. Woodland, The transition of orthoferrosilite to high-pressure C2/c clinoferrosilite at ambient temperature, *European Journal of Mineralogy* 8(1996) 1337-1345.
- [39] S.H. Shim, T.S. Duffy, G.Y. Shen, The stability and P-V-T equation of state of CaSiO₃ perovskite in the Earth's lower mantle, *Journal Of Geophysical Research-Solid Earth* 105(2000) 25955-25968.
- [40] Y. Wang, D.J. Weidner, F. Guyot, Thermal equation of state of CaSiO (sub 3) perovskite, *J.Geophys.Res.* 101(1996) 661-672.
- [41] B.B. Karki, J. Crain, First-principles determination of elastic properties of CaSiO₃ perovskite at lower mantle pressures, *Geophysical Research Letters* 25(1998) 2741-2744.
- [42] C.R.S. Dasilva, B.B. Karki, L. Stixrude, R.M. Wentzcovitch, Ab initio study of the elastic behavior of MgSiO₃ ilmenite at high pressure, *Geophysical Research Letters* 26(1999) 943-946.
- [43] J.H. Gieske, G.R. Barsch, Pressure Dependence of Elastic Constants of Single Crystalline Aluminum Oxide, *Physica Status Solidi* 29(1968) 121-131.
- [44] S.V. Sinogeikin, J.D. Bass, Single-crystal elasticity of pyrope and MgO to 20 GPa by Brillouin scattering in the diamond cell, *Physics of the Earth and Planetary Interiors* 120(2000) 43-62.
- [45] L. Thieblot, J. Roux, P. Richet, High-temperature thermal expansion and decomposition of garnets, *European Journal of Mineralogy* 10(1998) 7-15.
- [46] S.V. Sinogeikin, J.D. Bass, Elasticity of pyrope and majorite-pyrope solid solutions to high temperatures, *Earth and Planetary Science Letters* 203(2002) 549-555.

- [47] S.V. Sinogeikin, J.D. Bass, A. Kavner, R. Jeanloz, Elasticity of natural majorite and ringwoodite from the Catherwood meteorite, *Geophysical Research Letters* 24(1997) 3265-3268.
- [48] L. Zhang, H. Ahsbahs, A. Kutoglu, C.A. Geiger, Single-crystal hydrostatic compression of synthetic pyrope, almandine, spessartine, grossular and andradite garnets at high pressures, *Physics and Chemistry of Minerals* 27(1999) 52-58.
- [49] B. O'Neill, J.D. Bass, J.R. Smyth, M.T. Vaughan, Elasticity of a Grossular-Pyrope-Almandine Garnet, *Journal of Geophysical Research-Solid Earth and Planets* 94(1989) 17819-17824.
- [50] P.G. Conrad, C.S. Zha, H.K. Mao, R.J. Hemley, The high-pressure, single-crystal elasticity of pyrope, grossular, and andradite, *American Mineralogist* 84(1999) 374-383.
- [51] S.V. Sinogeikin, J.D. Bass, Elasticity of Majorite and a Majorite-Pyrope solid solution to high pressure: Implications for the Transition Zone, *Geophysical Research Letters* 29(2002).
- [52] D.J. Weidner, J.D. Bass, A.E. Ringwood, W. Sinclair, The single-crystal elastic moduli of stishovite, *Journal of Geophysical Research* 87(1982) 4740-4746.
- [53] D. Andrault, R.J. Angel, J.L. Mosenfelder, T. Le Bihan, Equation of state of stishovite to lower mantle pressures, *American Mineralogist* 88(2003) 301-307.
- [54] J. Liu, J.Z. Zhang, L. Flesch, B.S. Li, D.J. Weidner, R.C. Liebermann, Thermal equation of state of stishovite, *Physics of the Earth and Planetary Interiors* 112(1999) 257-266.
- [55] S.V. Sinogeikin, J.Z. Zhang, J.D. Bass, Elasticity of single crystal and polycrystalline MgSiO₃ perovskite by Brillouin spectroscopy, *Geophysical Research Letters* 31(2004).
- [56] R.M. Wentzcovitch, B.B. Karki, M. Cococcioni, S. de Gironcoli, Thermoelastic properties of MgSiO₃-perovskite: Insights on the nature of the Earth's lower mantle, *Physical Review Letters* 92(2004).
- [57] S.H. Shim, T.S. Duffy, Constraints on the P-V-T equation of state of MgSiO₃ perovskite, *American Mineralogist* 85(2000) 354-363.
- [58] G. Fiquet, A. Dewaele, D. Andrault, M. Kunz, T.L. Bihan, Thermoelastic properties and crystal structure of MgSiO₃ perovskite at lower mantle pressure and temperature conditions, *Geophysical Research Letters* 27(2000) 21-24.
- [59] B. Kiefer, L. Stixrude, R.M. Wentzcovitch, Elasticity of (Mg,Fe)SiO₃-Perovskite at high pressures, *Geophysical Research Letters* 29(2002).
- [60] A. Kubo, M. Akaogi, Post-garnet transitions in the system Mg₄Si₄O₁₂-Mg₃Al₂Si₃O₁₂ up to 28 GPa: phase relations of garnet, ilmenite and perovskite, *Physics of the Earth and Planetary Interiors* 121(2000) 85-102.
- [61] K.T. Thompson, R.M. Wentzcovitch, M.S.T. Bukowinski, Polymorphs of alumina predicted by first principles: Putting pressure on the ruby scale, *Science* 274(1996) 1880-1882.
- [62] I. Jackson, S.K. Khanna, A. Revcolevschi, J. Berthon, Elasticity, Shear-Mode Softening and High-Pressure Polymorphism of Wustite (Fe_{1-X}O), *Journal of Geophysical Research-Solid Earth and Planets* 95(1990) 21671-21685.
- [63] S.D. Jacobsen, H.J. Reichmann, H.A. Spetzler, S.J. Mackwell, J.R. Smyth, R.J. Angel, C.A. McCammon, Structure and elasticity of single-crystal (Mg,Fe)O and

- a new method of generating shear waves for gigahertz ultrasonic interferometry, *Journal of Geophysical Research-Solid Earth* 107(2002).
- [64] S. Stolen, R. Glockner, F. Gronvold, T. Atake, S. Izumisawa, Heat capacity and thermodynamic properties of nearly stoichiometric wustite from 13 to 450 K, *American Mineralogist* 81(1996) 973-981.

Table 1. Properties of mantle species.

Phase	Species	Formula	F_0 kJ mol ⁻¹	V_0 cm ³ mol ⁻¹	K_0 GPa	K'_0	θ_0 K	γ_0	q	G_0 GPa	G'_0	η_{SO}	W kJ mol ⁻¹	Ref.
feldspar (plg)	Anorthite	CaAl ₂ Si ₂ O ₈	-4006 (22)	100.61	84 (5)	4.0 (10)	752 (2)	0.39 (5)	1.0 (10)	40 (3)	1.1 (5)	1.6 (10)		[1-5]
spinel (sp)	Spinel	(Mg ₃ Al)(Al ₇ Mg)O ₁₆	-8666 (28)	159.05	197 (1)	5.7 (2)	878 (247)	1.02 (4)	2.8 (6)	109 (10)	0.4 (5)	2.7 (6)	5.0 (40)	[1,4,6-8]
spinel	Hercynite	(Fe ₃ Al)(Al ₇ Fe)O ₁₆	-7312 (35)	163.37	209 (2)	5.7 (10)	768 (23)	1.21 (7)	2.8 (10)	85 (13)	0.4 (5)	2.8 (10)		[1,2,4,9,10]
olivine (ol)	Forsterite	Mg ₂ SiO ₄	-2055 (2)	43.60	128 (2)	4.2 (2)	809 (1)	0.99 (3)	2.1 (2)	82 (2)	1.4 (1)	2.4 (1)	5.3 (38)	[1,4,8,11,12]
olivine	Fayalite	Fe ₂ SiO ₄	-1379 (2)	46.29	135 (2)	4.2 (10)	619 (2)	1.06 (7)	3.6 (10)	51 (2)	1.4 (5)	1.1 (6)		[1,2,4,5,8,13,14]
wadsleyite (wa)	Mg-Wadsleyite	Mg ₂ SiO ₄	-2027 (1)	40.52	169 (3)	4.3 (2)	849 (4)	1.21 (9)	2.0 (10)	112 (2)	1.4 (2)	2.7 (4)	6.1 (71)	[1,5,15-18]
wadsleyite	Fe-Wadsleyite	Fe ₂ SiO ₄	-1370 (10)	42.80	169 (13)	4.3 (10)	656 (27)	1.21 (30)	2.0 (10)	72 (12)	1.4 (5)	1.1 (10)		[15,19]
ringwoodite (ri)	Mg-Ringwoodite	Mg ₂ SiO ₄	-2018 (2)	39.49	183 (2)	4.1 (2)	889 (6)	1.09 (10)	2.8 (4)	120 (2)	1.3 (1)	2.7 (5)	3.5 (38)	[1,5,15,20]
ringwoodite	Fe-Ringwoodite	Fe ₂ SiO ₄	-1365 (2)	41.86	199 (7)	4.1 (10)	648 (8)	1.17 (22)	2.8 (10)	95 (10)	1.3 (5)	2.1 (10)		[15,20-22]
orthopyroxene (opx)	Enstatite	Mg ₉ Si ₄ O ₁₂	-5827 (6)	125.35	107 (2)	7.0 (4)	809 (8)	0.89 (4)	0.3 (11)	77 (1)	1.6 (1)	2.1 (5)		[1,4,23-27]
orthopyroxene	Ferrosilite	Fe ₄ Si ₄ O ₁₂	-4453 (8)	131.88	100 (4)	7.0 (5)	653 (14)	0.75 (8)	0.3 (10)	52 (5)	1.6 (5)	1.0 (10)		[1,2,4,23,28,29]
orthopyroxene	Mg-Tschermak's	(Mg ₂ Al ₂)Si ₂ Al ₂ O ₁₂	-6005 (19)	120.50	107 (10)	7.0 (10)	833 (27)	0.89 (30)	0.3 (10)	89 (10)	1.6 (5)	2.1 (10)		[30]
clinopyroxene (cpx)	Diopside	Ca ₂ Mg ₂ Si ₄ O ₁₂	-6060 (6)	132.08	112 (5)	5.2 (18)	782 (5)	0.96 (5)	1.5 (20)	67 (2)	1.4 (5)	1.6 (10)	26.3 (30)	[1,2,4,5,31,32]
clinopyroxene	Hedenbergite	Ca ₂ Fe ₂ Si ₄ O ₁₂	-5353 (50)	135.73	119 (4)	5.2 (10)	702 (4)	0.93 (6)	1.5 (10)	61 (1)	1.2 (5)	1.6 (10)		[1,2,4,5,14]
clinopyroxene	Mg-Diopside	Mg ₂ Mg ₂ Si ₄ O ₁₂	-5796 (14)	126.00	112 (10)	5.2 (10)	782 (14)	0.96 (30)	1.5 (10)	76 (10)	1.6 (5)	1.6 (10)		[33]
HP-clinopyroxene (hpcpx)	HP-Clinoenstatite	Mg ₉ Si ₄ O ₁₂	-5811 (6)	121.52	121 (1)	5.5 (3)	824 (7)	1.16 (5)	0.8 (5)	90 (1)	1.5 (1)	2.4 (5)		[34,35]
HP-clinopyroxene	HP-Clinoferrosilite	Fe ₄ Si ₄ O ₁₂	-4447 (8)	127.59	121 (10)	5.5 (10)	672 (11)	1.16 (30)	0.8 (10)	71 (10)	1.5 (5)	1.1 (10)		[36]
Ca-perovskite (cpv)	Ca-Perovskite	CaSiO ₃	-1447 (5)	27.45	236 (4)	3.9 (2)	725 (28)	1.47 (7)	1.7 (16)	165 (12)	2.5 (5)	2.2 (10)		[1,37-39]
akimotoite (ak)	Mg-Akimotoite	MgSiO ₃	-1406 (1)	26.35	211 (4)	4.5 (5)	912 (5)	1.21 (13)	1.3 (10)	132 (8)	1.6 (5)	2.7 (10)	66 (5)	[1,2,5,40]
akimotoite	Fe-Akimotoite	FeSiO ₃	-1046 (29)	26.85	211 (10)	4.5 (10)	725 (118)	1.21 (30)	1.3 (10)	157 (10)	1.6 (5)	3.5 (10)		[41]
akimotoite	Corundum	AlAlO ₃	-1583 (4)	25.58	253 (5)	4.3 (2)	933 (3)	1.32 (4)	1.3 (2)	163 (2)	1.6 (1)	2.8 (2)		[1,4,5,8,42]
gamet (gt,mj)	Pyrope	Mg ₃ AlAlSi ₃ O ₁₂	-5928 (5)	113.08	170 (2)	4.1 (3)	823 (4)	1.01 (6)	1.4 (5)	94 (2)	1.3 (2)	1.0 (3)		[1,4,43-45]
gamet	Almandine	Fe ₃ AlAlSi ₃ O ₁₂	-4940 (11)	115.43	177 (3)	4.1 (3)	742 (5)	1.10 (6)	1.4 (10)	98 (3)	1.3 (5)	2.2 (10)		[1,4,44,46,47]
gamet	Grossular	Ca ₃ AlAlSi ₃ O ₁₂	-6258 (56)	125.12	167 (1)	5.5 (4)	826 (2)	1.08 (6)	0.4 (4)	108 (1)	1.1 (2)	2.4 (2)		[1,4,8,44,48,49]
gamet	Mg-Majorite	Mg ₃ MgSi ₃ O ₁₂	-5691 (5)	114.32	165 (3)	4.2 (3)	825 (4)	0.97 (7)	1.5 (5)	85 (2)	1.4 (2)	0.8 (3)		[1,45,50,51]
stishovite (st)	Stishovite	SiO ₂	-811 (2)	14.02	314 (8)	4.4 (2)	1021 (21)	1.33 (17)	2.4 (22)	220 (12)	1.6 (5)	5.0 (10)		[1,5,52-54]
perovskite (pv)	Mg-Perovskite	MgSiO ₃	-1362 (1)	24.45	251 (3)	4.1 (1)	888 (4)	1.44 (5)	1.4 (5)	175 (2)	1.7 (2)	2.6 (6)	12 (5)	[1,55-59]
perovskite	Fe-Perovskite	FeSiO ₃	-1009 (3)	25.40	281 (40)	4.1 (10)	700 (10)	1.44 (30)	1.4 (10)	138 (40)	1.7 (5)	2.0 (10)		[60,61]
perovskite	Al-Perovskite	AlAlO ₃	-1518 (7)	25.49	228 (10)	4.1 (5)	903 (36)	1.44 (30)	1.4 (10)	159 (10)	1.7 (5)	2.9 (10)		[62,63]
magnesiowüstite (mw)	Periclase	MgO	-569 (1)	11.24	161 (3)	3.9 (2)	773 (9)	1.50 (2)	1.5 (2)	130 (3)	2.2 (1)	2.3 (2)	13.0 (20)	[1,4,7,8,43]
magnesiowüstite	Wüstite	FeO	-245 (1)	12.26	179 (1)	4.9 (2)	417 (7)	1.53 (13)	1.5 (10)	47 (1)	0.7 (1)	0.6 (10)		[5,64,65]